Institute of Space and Aeronautical Science, University of Tokyo
Report No. 566, December 1978

Flow and Temperature Fields around a Heated Circular Cylinder in a Fluctuating Flow of Low Reynolds Number—A Numerical Study on Thermo-Fluiddynamic Response of the Hot-Wire*

By

Tomio OBOKATA**, Atsushi OKAJIMA***, and Yoshimichi TANIDA

Summary: The purpose of the present paper is to elucidate the thermo-fluiddynamic characteristics of the constant-temperature hot-wire anemometer by a numerical calculation. Solving the vorticity and energy equations by an implicit difference approximation, obtained are the flow patterns and isotherms around a heated circular cylinder in a fluctuating flow for the time-mean flow of $Re=4$ and 40. The drag force and the rates of heat transfer from the cylinder are then determined. Their dependence on the amplitude and frequency of flow fluctuations are discussed, remarking the validity of the quasi-steady approximation.

1. INTRODUCTION

The constant-temperature hot-wire anemometer is utilized as one of the most common devises for the measurement of flow velocity. Its characteristic that is the so-called frequency response has been studied by many investigators especially in the case where the fluctuations in flow were sufficiently small as compared with the time-mean flow. The investigations made so far, however, are almost concerned with the estimation and improvement of the frequency response of the hot-wire anemometer from the electronic engineering point of view, assuming that heat transfer from the hot-wire occurs in a quasi-steady manner over a moderate frequency range.

The heat transfer to and from a cylindrical body immersed in a fluctuating flow has also been noticed in connection with heat exchangers and turbine blades. Theoretical study on a fluctuating heat transfer of a periodic boundary layer on a cylindrical body has been made by, for example, Lighthill (1954), Mori & Tokuda (1966), Ishigaki (1970, 1972). The solutions thus obtained apply only at Reynolds number for which the boundary-layer approximation has some validity.

* The principal parts of this paper were published already in Transactions of the Japan Society of Mechanical Engineers, 43-367 (1977), 1103. (in Japanese)

** College of Technology, Gunma University.

*** Research Institute for Applied Mechanics, Kyushu University.

So far, for the hot-wire, the assumption of the quasi-steady characteristics for the flow and temperature fields around the heated wire has been considered to be valid, although no reliable theoretical and experimental proofs existed. Further, for more extended availability of the hot-wire anemometer, there will be encountered necessarily not only with the case where the fluctuations of much higher frequency should be searched out but also with the case where the velocity fluctuations are large enough such that reversed flow occurs inevitabley.

The purpose of the present paper is to elucidate the thermo-fluiddynamic characteristics of the hot-wire by a numerical calculation, remarking its dependence on the amplitude and frequency of flow fluctuation as well as the validity of the quasi-steady approximation.

2. Formulation of the Problem

Consider the motion of a viscous incompressible fluid around a stationary circular cylinder of radius a (see figure 1). Two-dimensional, symmetric case is considered,

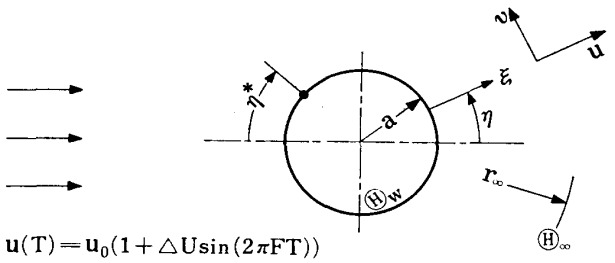

Fig. 1. Model and notation.

thereby precluding the possibility of the generation of the Kármán vortex street behind the cylinder. The surface of the cylinder is kept at a uniform temperature Θ_w, and the fluid which is infinitely far from the cylinder is at a uniform temperature $\Theta_\infty<\Theta_w$. The main stream velocity far from the cylinder oscillates sinusoidally at a frequency f with the dimensionless amplitude ΔU about a time-mean velocity u_0, that is expressed as $u=u_0(1+\Delta U \sin 2\pi ft)$.

All the fluid properties are taken as constant: density (ρ), kinematic viscosity (ν), and thermal diffusivity (κ). The following dimensionless quantities are introduced: time, $T=u_0t/a$; temperature, $\theta=(\Theta-\Theta_\infty)/(\Theta_w-\Theta_\infty)$; frequency, $F=af/u_0$; radial and circumferential components of velocity, $U=u/u_0$ and $V=v/u_0$. Further defined are the Reynolds number $Re=2au_0/\nu$ and the Prandtl number $Pr=\nu/\kappa$.

The physical polar coordinates (r, φ) is mapped onto an orthogonal coordinate system (ξ, η) by a transformation that $\xi=\ln(r/a)$ and $\eta=\varphi$. Eliminating pressure by taking the rotation of the momentum equations leads to the equation for vorticity

$$\frac{\partial\zeta}{\partial T}+\frac{1}{h}\left(U\frac{\partial\zeta}{\partial\xi}+V\frac{\partial\zeta}{\partial\eta}\right)=\frac{1}{Re}\frac{1}{h^2}\nabla^2\zeta, \qquad \nabla^2=\frac{\partial^2}{\partial\xi^2}+\frac{\partial^2}{\partial\eta^2} \tag{1}$$

where $h=e^\xi$ is the scale factor of this cooordinate system and ζ is the vorticity de-

fined as $\zeta=\{\partial(hV)/\partial\xi-\partial(hU)/\partial\eta\}/h^2$. The energy equation takes the form

$$\frac{\partial\theta}{\partial T}+\frac{1}{h}\left(U\frac{\partial\theta}{\partial\xi}+V\frac{\partial\theta}{\partial\eta}\right)=\frac{1}{RePr}\frac{1}{h^2}\nabla^2\theta \tag{2}$$

in the absence of viscous dissipation and radiation effects.

By introducing a dimensionless stream function ψ, the continuity equation is automatically satisfied, and the following relations are provided.

$$U=\frac{1}{h}\frac{\partial\psi}{\partial\eta},\qquad V=-\frac{1}{h}\frac{\partial\psi}{\partial\xi} \tag{3}$$

and

$$\nabla^2\psi=-h^2\zeta \tag{4}$$

Equations (1)–(4) are to be solved for ψ, ζ, and θ subject to specific initial conditions and boundary conditions. The boundary conditions for $T>0$ are: on the surface of the circular cylinder ($\xi=0$),

$$\psi=\frac{\partial\psi}{\partial\xi}=0,\qquad \theta=1 \tag{5}$$

and for the flow field infinitely far from the cylinder, where the velocity and temperature of the fluid asymptotically tends to the uniform values of free stream as the distance becomes infinite,

$$\psi_\infty=2(1+\Delta U\sin 2\pi FT)\sinh\xi\sin\eta,\qquad \zeta_\infty=\Theta_\infty=0. \tag{6}$$

In practical computation, however, the latter boundary conditions should be imposed on a far but finite boundary, which are taken in the present calculation $\xi=\pi$ and $3/2\pi$ or $r_\infty/a=23$ and 111 for $Re=4$ and 40, respectively.

The coefficients of the pressure and viscous shear stress on the surface of the cylinder are obtained by

$$\left.\begin{aligned} C_P(\eta)-C_P(0)&=\frac{4}{Re}\int_0^\eta\left(\frac{\partial\zeta}{\partial\xi}\right)_{\xi=0}d\eta\\ C_S(\eta)&=\frac{4}{Re}\zeta_{\xi=0}\end{aligned}\right\} \tag{7}$$

Then the coefficient of the drag force is

where

$$\left.\begin{aligned} C_D&=C_{DP}+C_{DS}\\ C_{DP}&=-\frac{1}{2}\int_0^{2\pi}C_P(\eta)\cos\eta\,d\eta\\ C_{DS}&=-\frac{1}{2}\int_0^{2\pi}C_S(\eta)\sin\eta\,d\eta\end{aligned}\right\} \tag{8}$$

The local heat transfer rate per unit area of the cylinder surface which is expressed by the dimensionless Nusselt number is

$$N_u = \left(\frac{\partial \theta}{\partial \xi}\right)_{\xi=0}. \tag{9}$$

The rate of the average heat transfer from the cylinder or the average Nusselt number is

$$N_{um} = \frac{1}{2\pi}\int_0^{2\pi} N_u d\eta. \tag{10}$$

3. Numerical Method

The governing partial differential equations for vorticity and energy are approximated by an implicit finite difference scheme. The numerical method which was developed by one of the authors (Okajima, Takata & Asanuma 1971) is applied as follows.

Approximate solutions of equations (1)–(4) will be obtained at a finite number of grid points in the (ξ, η)-plane for each discrete time. The (ξ, η)-plane is first divided into a finite discrete mesh of grid points having coordinates iS, jS where S is the grid spacing and i and j are integers. The circumference of the cylinder is cut into N equal parts, such that $S = 2\pi/N$. The gradation of mesh size is conveniently achieved by transforming the physical plane onto the (ξ, η)-plane. Just outside of the cylinder where the radial gradients of flow velocity and temperature are abrupt, the radial mesh is divided into two, $S/2$, in the range $r = a \sim r_f$. This finer mesh is certainly desirable in view of both the accuracy of computation and the economy of computing time.

Suppose that all quantities are known at a time T. By using implicit finite difference approximation to the vorticity and temperature equations, the vorticity and temperature at the next discrete time $T + \Delta T$ are obtained for all grid points except on the cylinder surface. The stream function which corresponds to the new vorticities is obtained from equation (4) by the method of successive over-relaxation. The new surface vorticities are then computed from the stream function in the vicinity of the cylinder. The above-mentioned procedures are repeated untill all quantities converge to reasonably accurate values at each time. Finally, drag coefficients and heat transfer rates can be determined from equations (7)–(10).

Table 1 gives the conditions adopted for the present calculation.

Table 1. Conditions for computation

Re	N	r_∞/a	r_f/a	ΔT
4	20	23	4.8	$\leqq 0.025$
40	40	111	1.9	$\leqq 0.05$

4. Results

The numerical calculations are carried out for Reynolds numbers $Re=4$ and 40, covering a range of fluctuating frequency from $F=0$ to 2.5 and that of the amplitude of flow fluctuation $\Delta U=0$ to 1.2. For example, the dimensionless frequency $F=0.01$ for $Re=4$ corresponds to the frequency $f=48$ kHz for the flow velocity $u_0=12$ m/s when the hot-wire of 5μ diameter is placed in an air stream. The Prandtl number is taken as 1.0 throughout the present calcualtion.

4.1 Case of Steady Flow

The flow patterns and temperature field around a circular cylinder in uniform steady flows are illustrated in figure 2. Only a symmetrical case being considered, sets of streamlines and isotherms are displayed in the upper and lower halves of the figure, respectively.

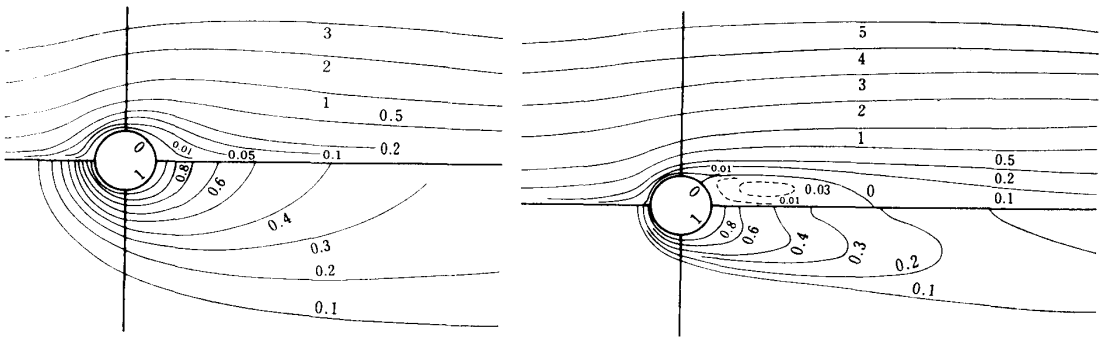

a) Re = 4 b) Re = 40

FIG. 2. Steady-state streamline (the upper half) and temperature (the lower half) fields. (a) $Re=4$, (b) $Re=40$.

The flow patterns at $Re=4$ agrees well with the previous numerical results (Keller & Takami 1960) revealing no separation of flow which results in the smooth configurations of isotherms. At $Re=40$, a pair of standing vortices are formed behind the cylinder, as was calculated by Apelt (1961), and then the isotherms reveal the defect of thermal wake behind the cylinder. Taking the local Nusselt number at the front stagnation point as unity, N_u drops along the surface to 0.25 at the separation point, but it falls only slowly in the region of the vortex pair (see figure 5 (*b*)), that is

TABLE 2. Calculated results for steady flow, in comparison with experimental results

Re	C_D		N_{um}	
	present calculation	Tritton's experiments	present calculation	McAdams' book
4	5.2	4.8	1.5	1.4
40	1.4	1.6	3.7	3.4

in contrast with the turbulent case when it recovers to 1 again at the rear stagnation point due to the recirculating vortex pair (Howarth 1953).

Table 2 gives the calculated results of the drag coefficient C_D and the average Nusselt number N_{um}, in comparison with the experimental results given by Tritton (1959) and in McAdams' book (1954), respectively.

4.2 *Case of Fluctuating Flow*

The flow and temperature fields in the case of a fluctuating flow are obtained by carrying the numerical calculation from the initial steady-state conditions which were already given in the previous section. The regular periodicity of the fluctuations in flow is nearly attained after the lapse of a few cyles of the fluctuations since the initial situation ($T=0$).

4.2.1 *Flow Patterns and Isotherms*

(i) Small Amplitude Case ($\Delta U=0.2$)

At $Re=4$, the flow and temperature fields of the flows fluctuating with the frequencies $F=0.025$ and 1.0 are illustrated in figure 3 only at the crest and trough phase of the fluctuating flow velocity, $\phi_U=90°$ and 270°.

The states at a lower frequency such as $F=0.025$ resemble closely the steady flow case in both flow and temperature fields. At $F=1.0$, the generation and release of the vortex pair are observed behind the cylinder in the deceralating phase ($\phi_U \fallingdotseq 160° \sim 315°$), whereas no marked variation in the temperature field appears over all the period.

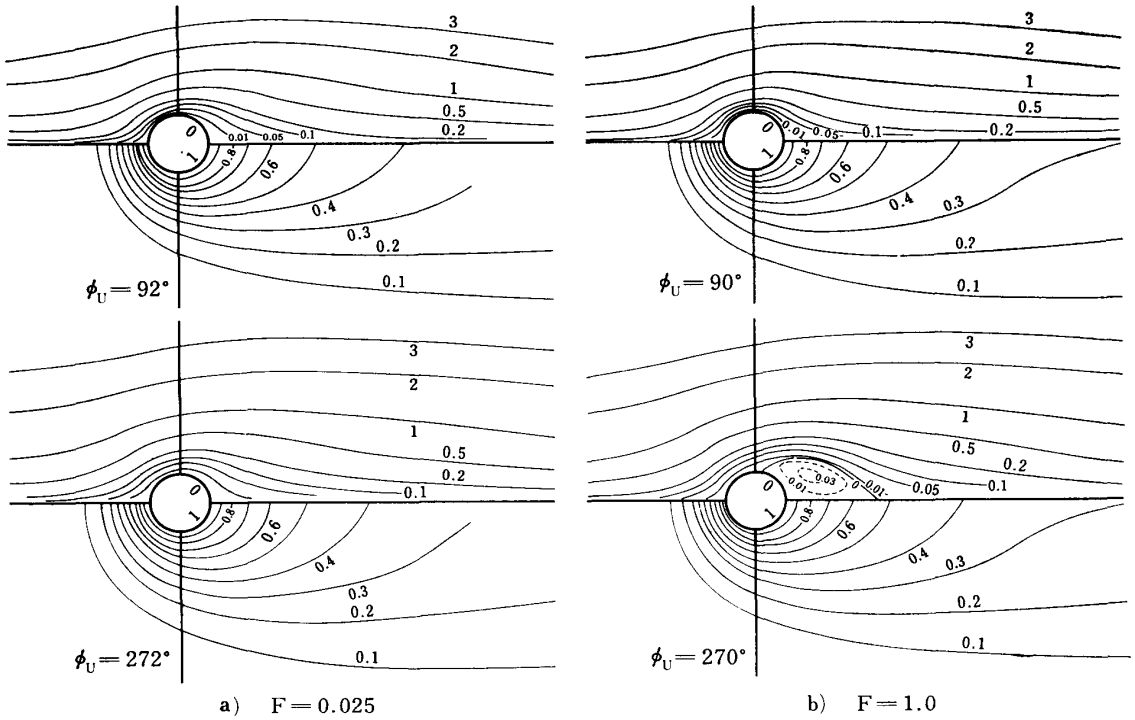

FIG. 3. Unsteady streamline (the upper half) and temperature (the lower half) fields. $\Delta U=0.2$, $Re=4$. (a) $F=0.025$, (b) $F=1.0$.

The flow and temperature fields of the fluctuating flows at $Re=40$ are illustrated in figure 4 for the frequencies $F=0.025$ and 0.25. At $F=0.025$, the vortex pair exists during all the period while growing and degenerating repeatedly; that is, in the accelerating phase the vortices diminish in size and the defect of the thermal wake

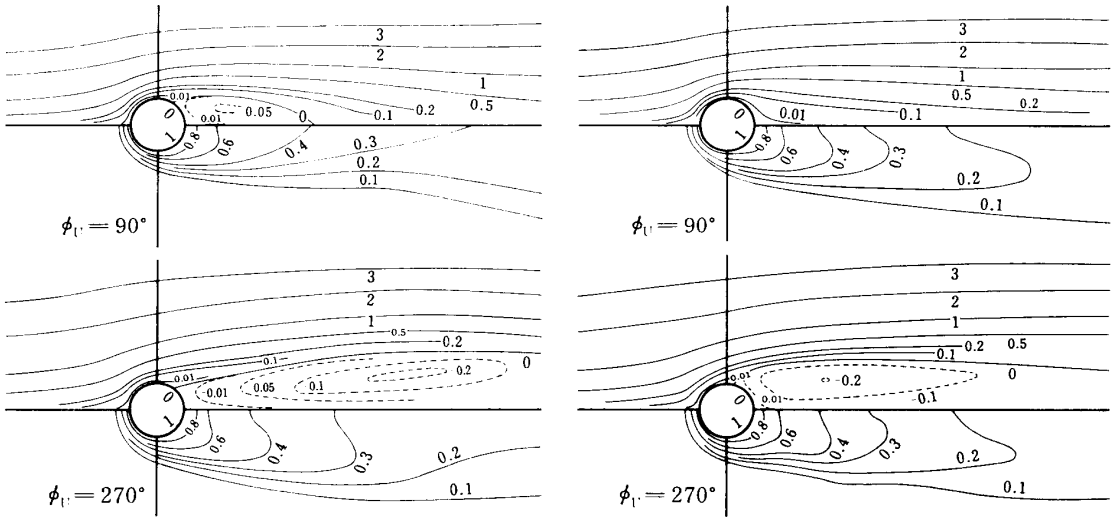

a) F = 0.025 b) F = 0.25

FIG. 4. Unsteady streamline (the upper half) and temperature (the lower half) fields. $\Delta U=0.2$, $Re=40$. (a) $F=0.025$, (b) $F=0.25$.

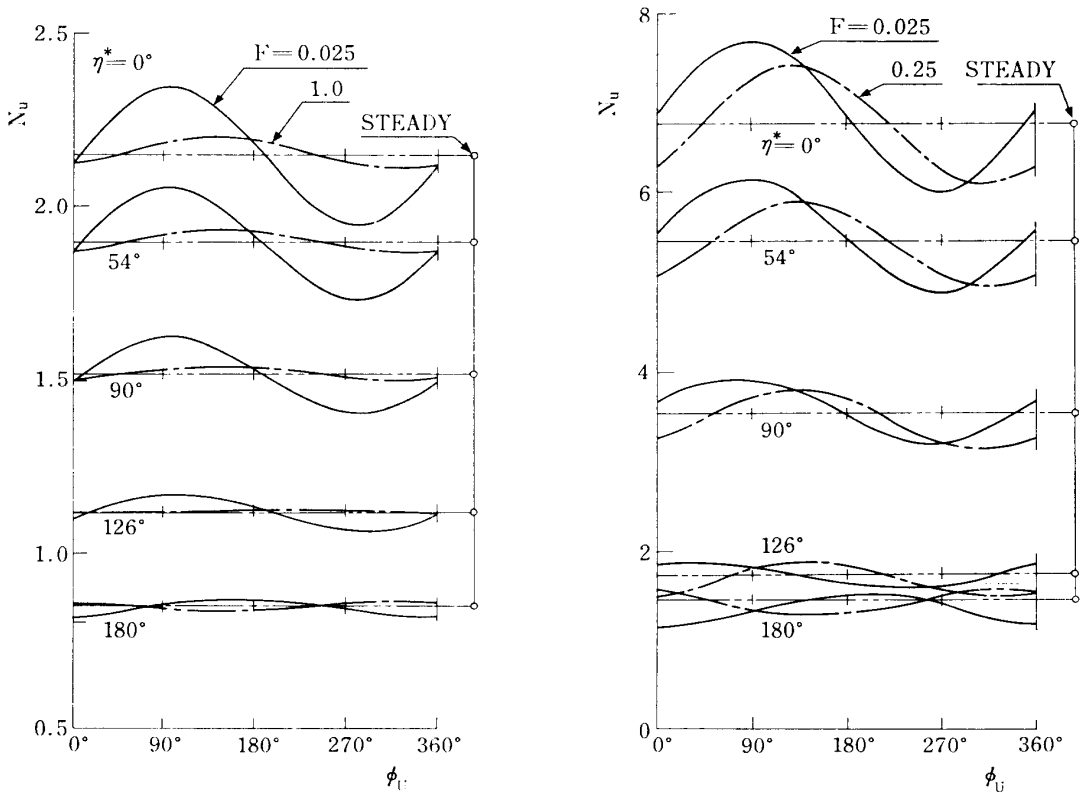

(a) (b)

FIG. 5. Local Nusselt number versus time. $\Delta U=0.2$. (a) $Re=4$, (b) $Re=40$.

disappears, while in the decelerating phase the vortices grow very large extending far downstream and the defect of the thermal wake appears. At a high frequency such as $F=0.25$, the vortex pair which is generated during the decelerating phase is released downstream during the accelerating phase, when the flow pattern in the vicinity of the cylinder is like that at much lower Reynolds number. The apparent defect of the thermal wake is obseved over all the period.

The variation of the rate of local heat transfer with time is nearly sinusoidal as

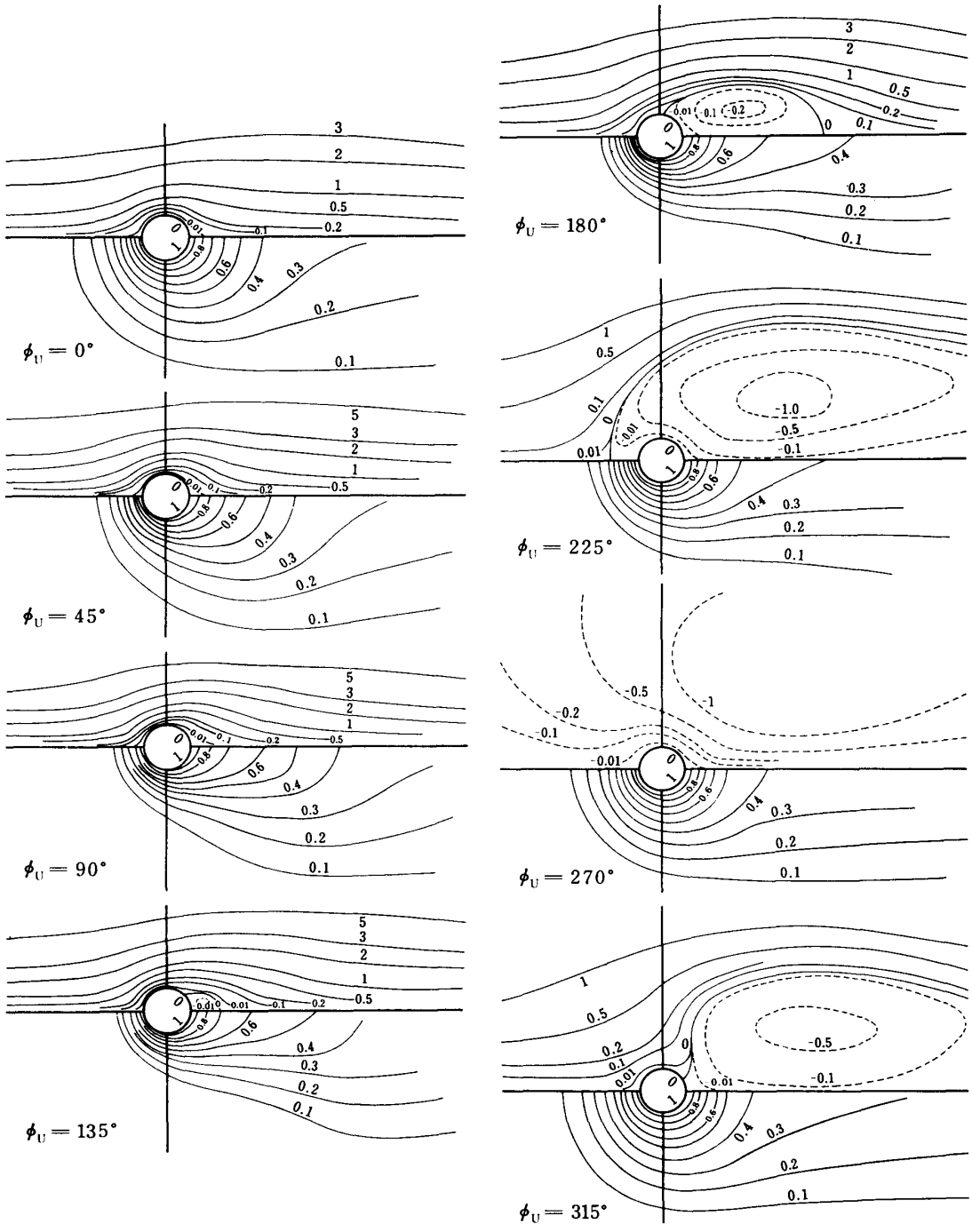

FIG. 6. Unsteady streamline (the upper half) and temperature (the lower half) fields. $\Delta U=1.0$, $Re=4$, $F=0.0833$.

illustrated in figure 5, where the parameter η^* is the coordinate along the cylinder surface from the front stagnation point (see figure 1). For higher fluctuating frequency, the local Nusselt number varies with larger phase lagging behind the fluctuating flow velocity and with small amplitude. No marked variation of the phase of the local Nusselt number against the fluctuating flow velocity exists in the front three-quarter region of the cylinder surface, but apparent phase reversal occurs at the back near the rear stagnation point, being attributed to the recirculating vortex pair.

(ii) Large Amplitude Case ($\Delta U = 1.0$)

The flow and temperature fields of the flow at $Re=4$ with the fluctuating frequency $F=0.0833$ are illustrated in figure 6. In the accelerating phase, no vortex pair is observed behind the cylinder, when the flow patterns and isotherms are almost similar to the steady case. The vortex pair begins to be formed as soon as the flow is decelerated. The vortex pair develops so strongly and abruptly that the cylinder is entirely embedded in the reversed wake flow at the phase of the minimum flow velocity ($\phi_U=270°$). This striking featre of the flow patterns is exmined by an experiment of flow visualization. Figure 7 presents a sequence of the photographs taken under the same conditions with figure 6. The experiment was performed by towing a circular cylinder of 30 *mm* diameter in a tank (0.7 *m* wide, 0.4 *m* deep, and 10 *m* long) which is filled with mobile oil. The cylinder is oscillated by a mechanical oscillator with the conditions corresponding to the flow fluctuation. The flow around the cylinder was visualized by floating Aluminium powder on the free surface and photographed by a camera which was fixed to the cylinder. Comparison of figure 7 with figure 6 shows that the flow patterns obtained agree quite well with each other.

The flow and temperature fields of the flows at $Re=40$ with the fluctuating frequency $F=0.025$ are illustrated in figure 8. In the accelerating phase, it is seen that the new vortex pair is being generated behind the cylinder immediately after the old

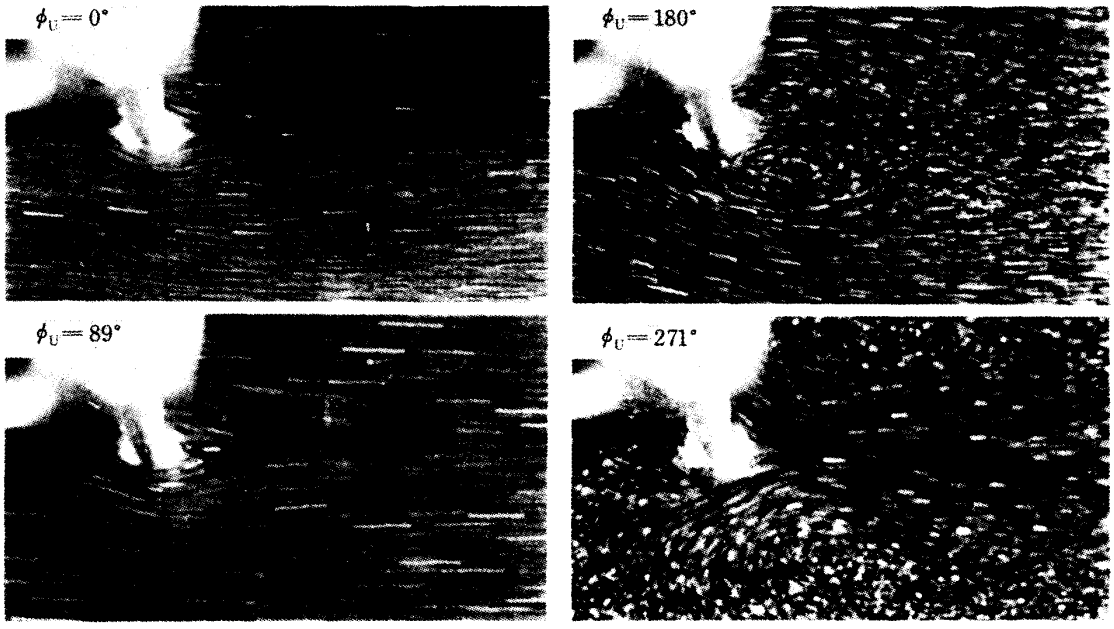

FIG. 7. Visualized flow patterns around a circular cylinder. $\Delta U=1.0$, $Re=4$, $F=0.076$.

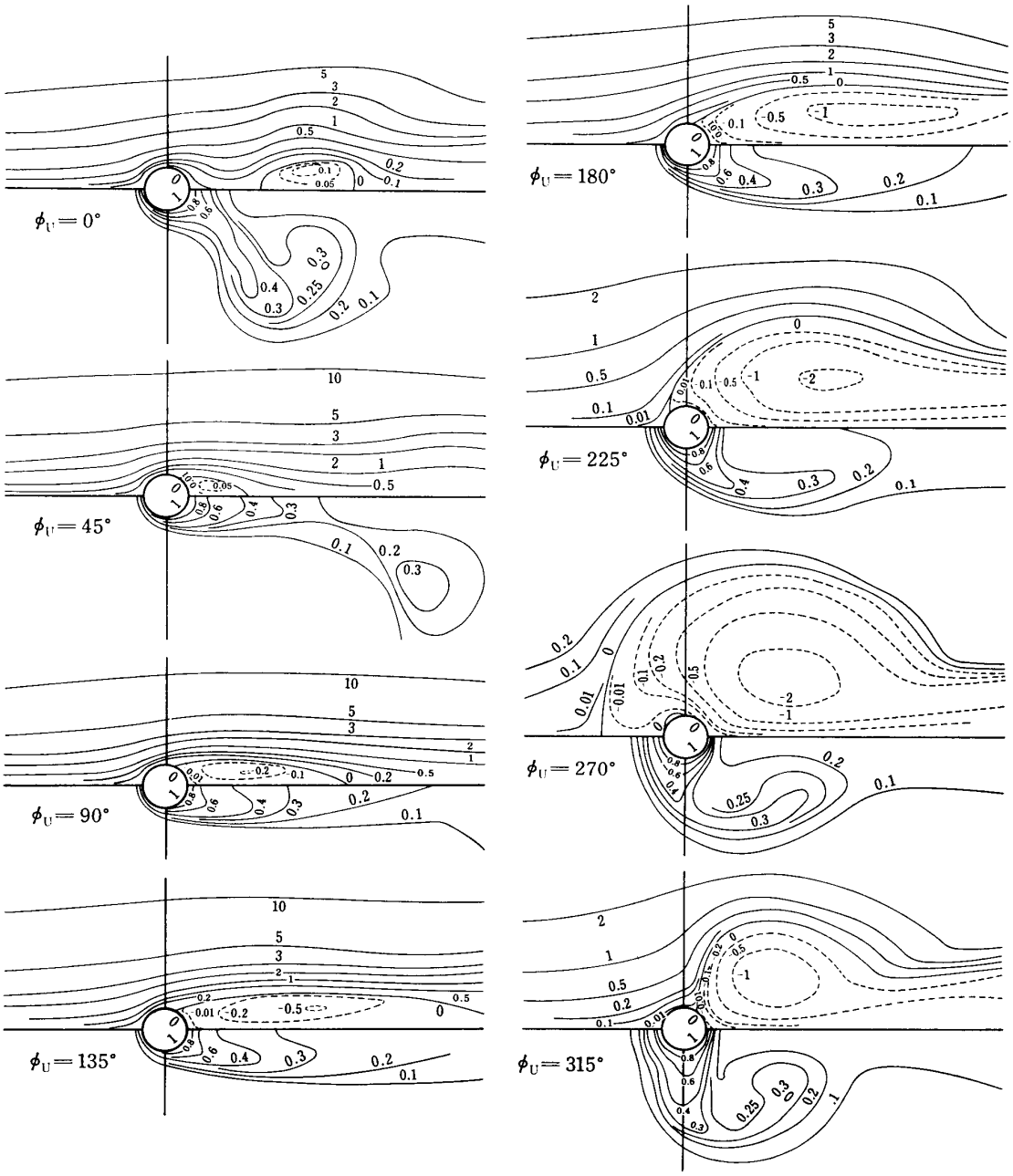

FIG. 8. Unsteady streamline (the upper half) and temperature (the lower half) fields. $\Delta U=1.0$, $Re=40$, $F=0.025$.

one is released downstream. Similarly as in the case of $Re=4$, the cylinder is entirely embedded in the reversed wake flow in the decelerating phase. The isotherms are much deformed according to the generation and degeneration of the wake vortices, so that the marked defect of the thermal wake appears especially in the decelerating phase.

The variation of the local Nusselt number with time is shown in figure 9. N_u in the vicinity of the rear stagnation point varies in anti-phase with others. This extraordinary feature can be attributed to the reversed wake flow at around $\phi_U=270°$,

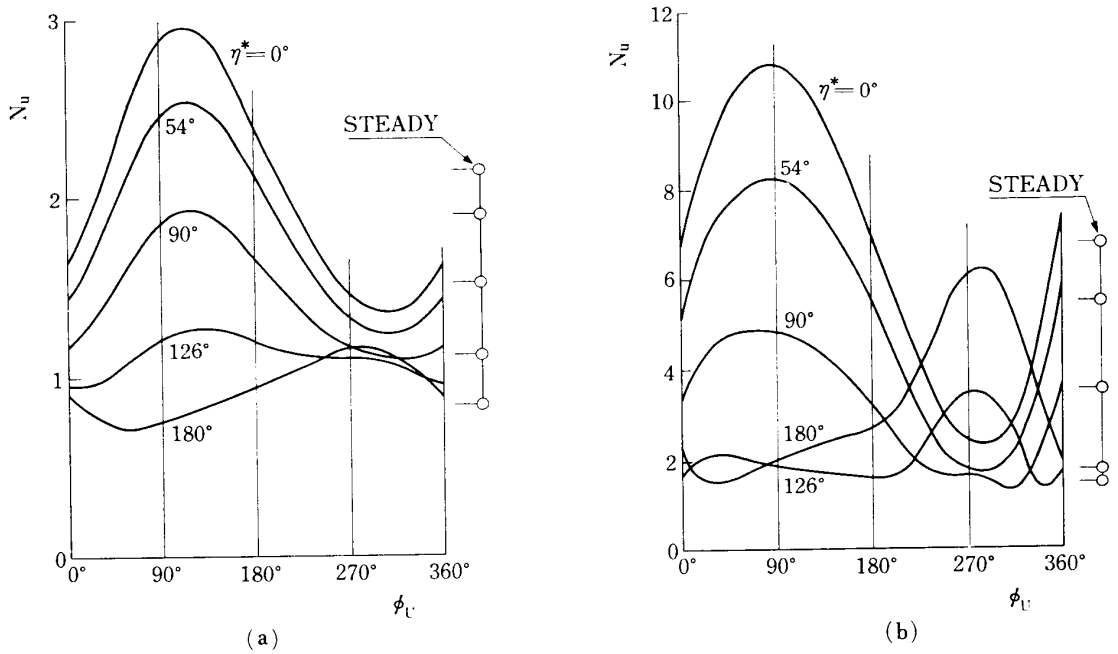

FIG. 9. Local Nusselt number versus time. $\Delta U=1.0$. (a) $Re=4$, $F=0.0833$ (b) $Re=40$, $F=0.025$.

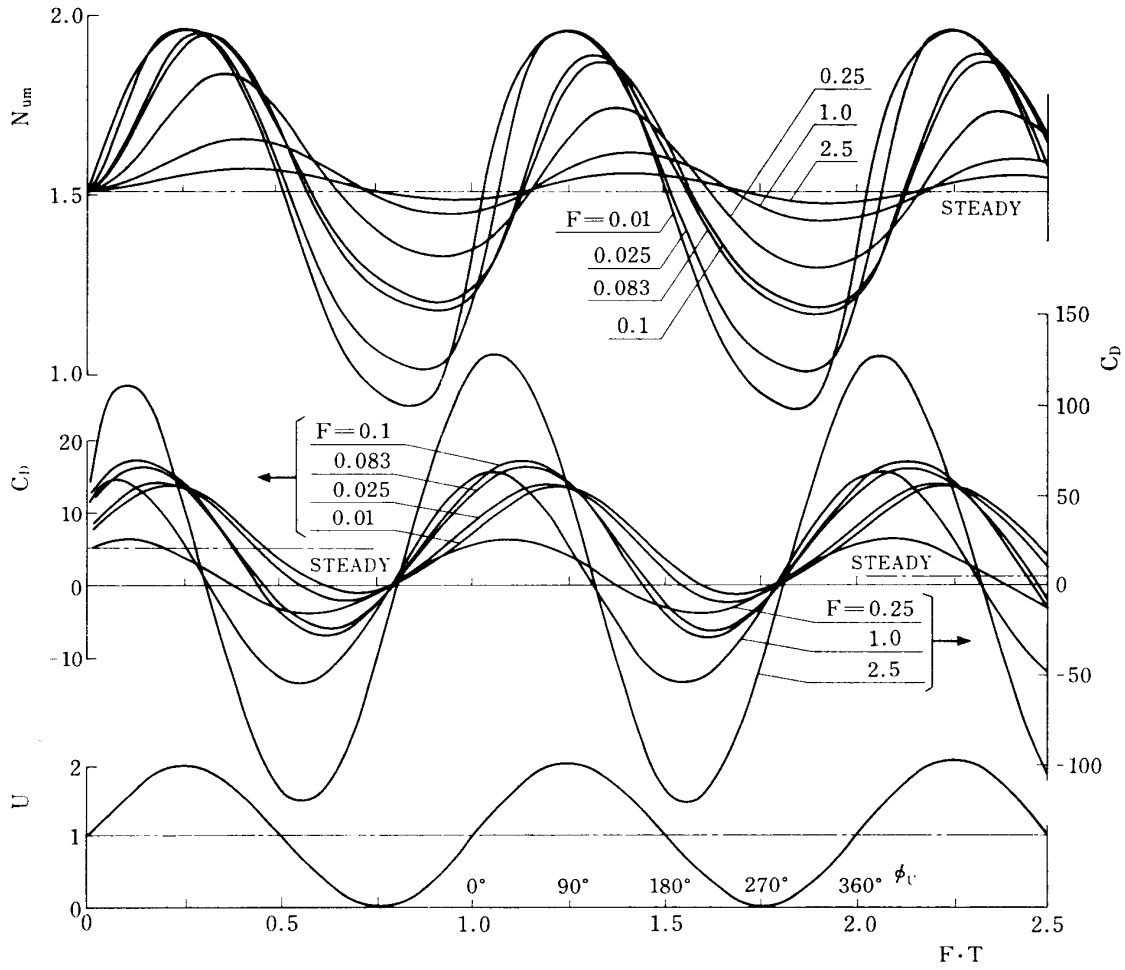

FIG. 10. Average Nusselt number and drag coefficient versus time. $\Delta U=1.0$, $Re=4$.

when the rear stagnation point behaves like the front stagnation point in the reversed flow and the heat transfer over rear half of the cylinder becomes prevailing.

4.2.2 *Heat Transfer Rates and Drag Force*

When the velocity fluctuation is much smaller than the time-mean velocity, both of the heat transfer rates and drag force vary in nearly sinusoidal manner with the amplitude proportional to the velocity amplitude (see figure 15). So, only the time-variation of the average Nusselt number and the drag coefficient for $\Delta U=1.0$ are presented here in figures 10 and 11, for $Re=4$ and 40 respectively. Only a few cycles of the period elapses before regular periodicity is nearly attained.

Figures 10 and 11 shows that at lower fluctuating frequency the waveform of N_{um} is markedly deformed in the phase of the low flow velocity, whereas at higher frequency it varies in sinusoidal manner with reduced amplitude lagging much behind the fluctuating flow velocity. This deformed waveform of N_{um} is attributable to the reversed wake flow which embeds the cylinder and promotes the heat transfer at the back of the cylinder.

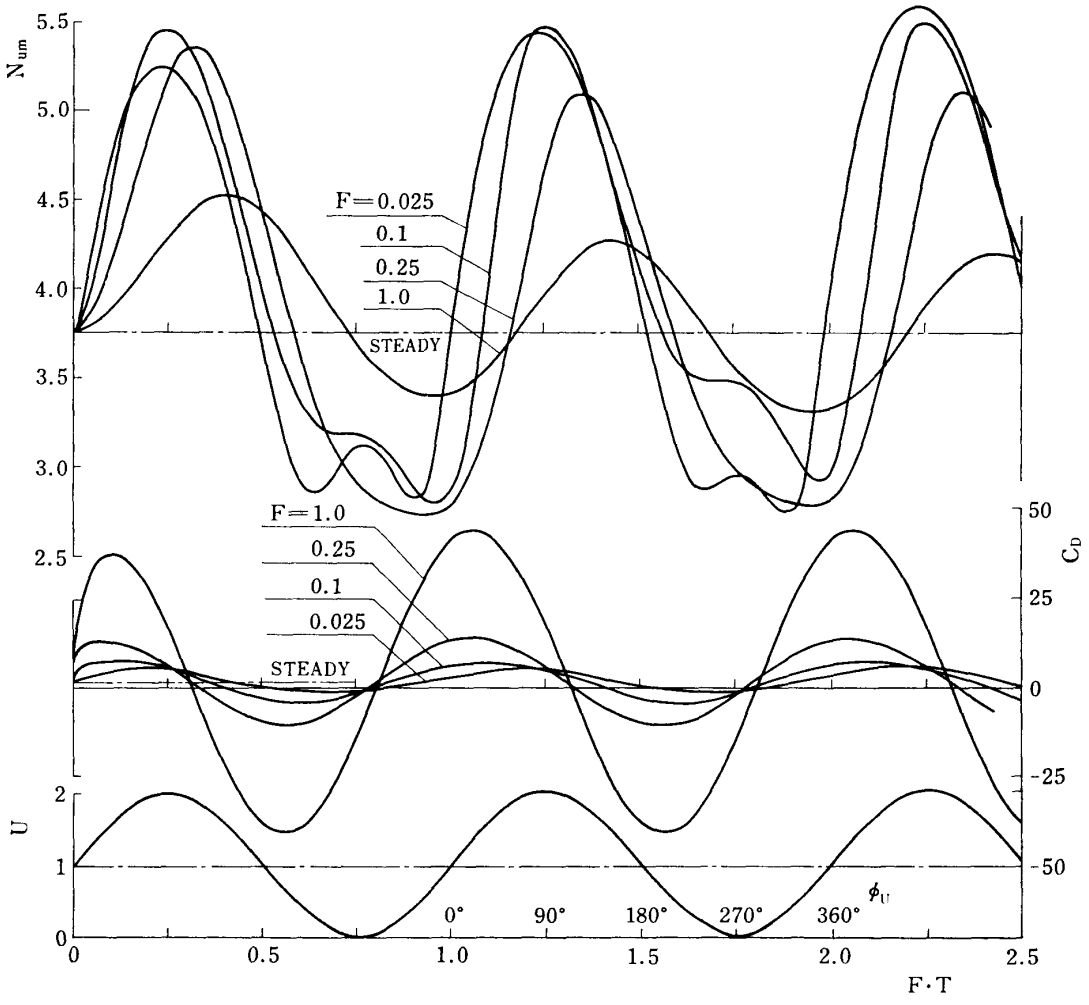

FIG. 11. Average Nusselt number and drag coefficient versus time. $\Delta U=1.0$, $Re=40$.

4.2.3 Frequency Dependence of Heat Transfer Rates and Drag Force

The frequency dependence of the average heat transfer rate and the drag force are obtained from their waveform discussed in the previous section.

(i) Small Amplitude Case ($\Delta U=0.2$)

The amplitude of the average Nusselt number $\tilde{N}_{um}$ and its phase angle ϕ_N (relative to ϕ_U) as a function of the fluctuating frequency are presented in figure 12. The

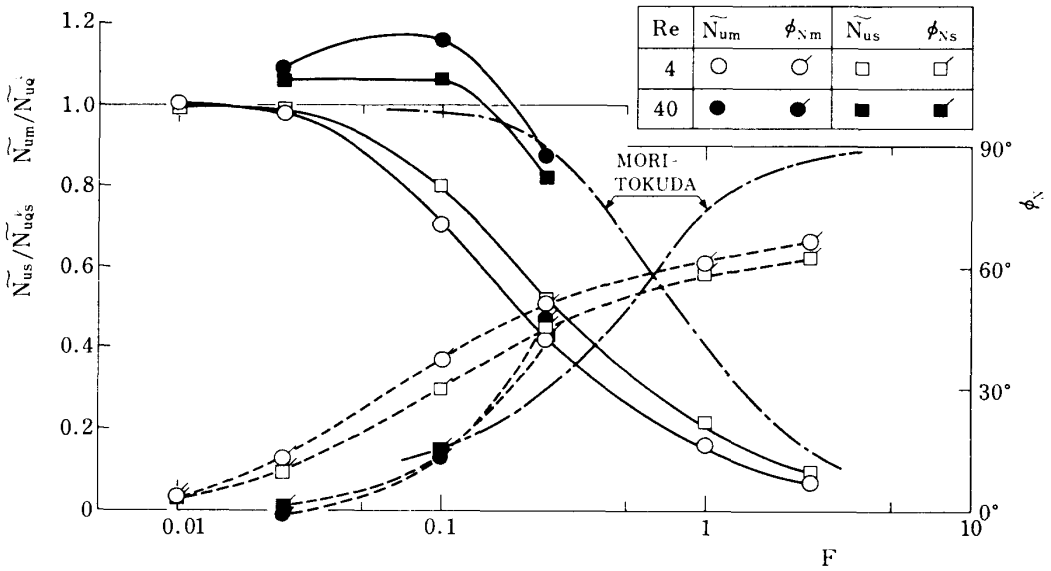

FIG. 12. Frequency response of Nusselt numbers. $\Delta U=0.2$.

amplitude of the local Nusselt number at the front stagnation point $\tilde{N}_{uS}$ is also given in this figure. The ordinate is the ratio $\tilde{N}_u/\tilde{N}_{uQ}$, where $\tilde{N}_{uQ}$ is the quasi-steady Nusselt number presumed from the steady values corresponding to the maximum and minimum of the fluctuating velocity. Both $\tilde{N}_{um}$ and $\tilde{N}_{us}$ vary in similar tendency at each Reynolds number. Define the critical frequency at which the amplitude of the Nusselt number deteriorates by 5% below the quasi-steady value, that is $\tilde{N}_u/\tilde{N}_{uQ} \leqq 0.95$. The critical frequencies at $Re=4$, 0.033 and 0.04 for $\tilde{N}_{um}$ and $\tilde{N}_{uS}$ respectively, are much lower than those at $Re=40$.

At $Re=40$, an overshoot of the amplitude of the average Nusselt number, $\tilde{N}_u/\tilde{N}_{uQ} > 1.0$, appears in the lower frequency range, which may be attributed to the unsteady behaviour of the vortex pair. For comparison, theoretical results for the local Nusselt number at the front stagnation point which were obtained by the boundary-layer approximation (Mori & Tokuda 1966) are presented by dot-dash lines in this figure. The agreement between theory and numerical calculation is rather encouraging.

Figure 13 shows the amplitude of the drag coefficient $\tilde{C}_D$ and its phase angle ϕ_D (relative to ϕ_U) as a function of the fluctuating frequency. The drag coefficient is divided into the pressure and friction components, ($\tilde{C}_{DP}$, ϕ_{DP}) and ($\tilde{C}_{DS}$, ϕ_{DS}), which are also presented in this figure. The ordinate is the ratio $\tilde{C}_D/\tilde{C}_{DQ}$, where $\tilde{C}_{DQ}$ is the quasi-steady drag amplitude which is presumed from the steady characteristics. The amplitude of any drag coefficient increases with increasing frequency. For suffi-

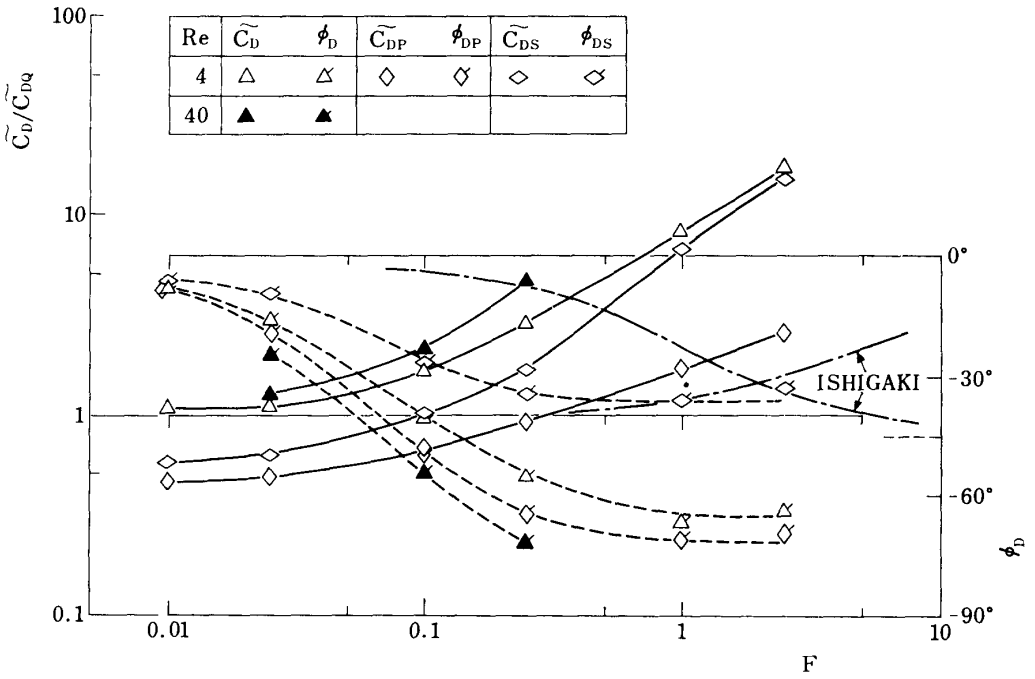

FIG. 13. Frequency response of drag coefficients. $\Delta U=0.2$.

ciently high frequency, the pressure drag overwhelms the friction drag as the effect of the virtual mass of fluid compels $\tilde{C}_{DP}$ to be proportional to the fluctuating frequency F with negative phase lag $\phi_{DP}=-90°$, whereas $\tilde{C}_{DS}$ tends to be proportional to $F^{1/2}$ with $\phi_{DS}=-45°$.

(ii) Large Amplitude Case ($\Delta U=1.0$)

In the large amplitude case when the cylinder experiences the reverse flow during a part of the cycle, the waveforms of the Nusselt number and the drag force are so deformed that their time-variations must be evaluated by taking the root-mean-square value. Figure 14 shows the r.m.s. values of the average Nusselt number and the drag coefficient as a function of the fluctuating frequency. The ordinate is the ratio

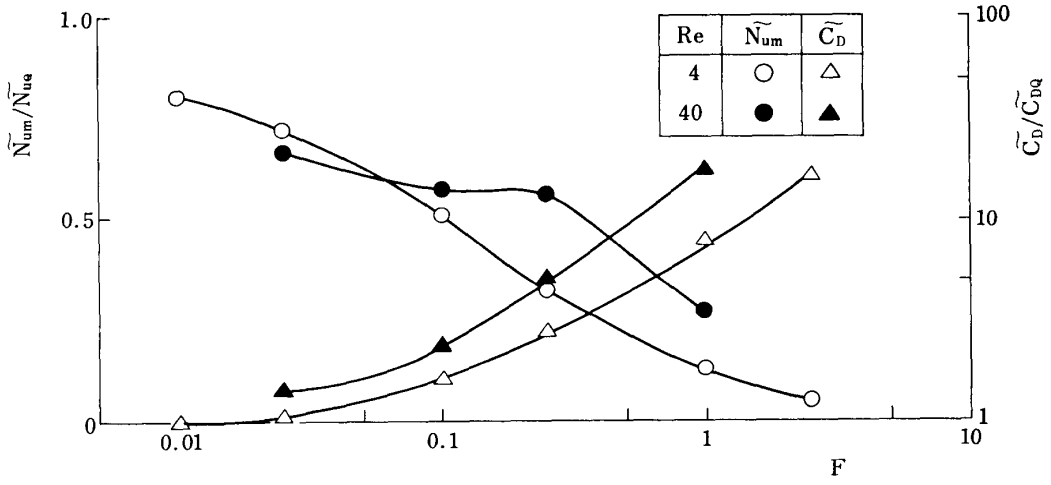

FIG. 14. Frequency response of Nusselt number and drag coefficient. $\Delta U=1.0$.

$\tilde{N}_{um}/\tilde{N}_{uQ}$ or $\tilde{C}_D/\tilde{C}_{DQ}$, where $\tilde{N}_{uQ}$ is the quasi-steady r.m.s. value presumed from the empirical relation $N_{um}=0.42+0.57\sqrt{Re}$ (Hinze 1959) and $\tilde{C}_{DQ}$ is the quasi-steady r.m.s. value presumed by assuming that C_D varies along the Trition's (1959) experimental curve.

Figure 14 shows that the amplitude ratio of the average Nusselt number is much smaller than unity even in a rather low frequency range, even though the trends with the frequency are similar to the small amplitude case. That is because the waveform which is deformed by the reversed wake flow is entirely different from the quasi-steady one even in the low frequency range.

4.3.3 Amplitude Dependence of Heat Transfer Rates and Drag Force

The average Nusselt number and the drag coefficient depend on the amplitude of the fluctuating flow velocity not only in their amplitudes but also in their waveforms, as shown in figure 15 for $Re=4$ at $F=0.025$,.

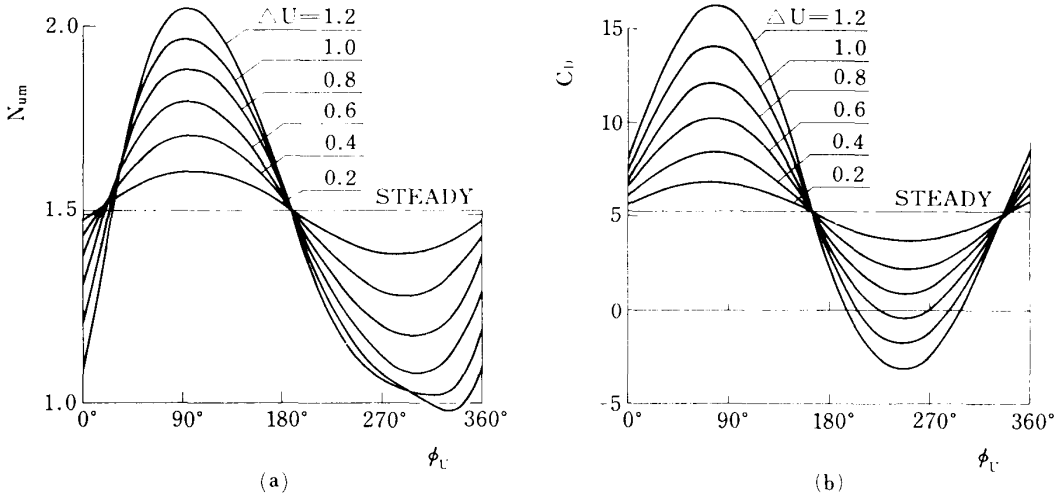

FIG. 15. Average Nusselt number and drag coefficient for various amplitudes of fluctuating flow velocity. $Re=4$, $F=0.025$.

For the velocity amplitude much smaller than $\Delta U=1.0$, both of the average Nusselt number and the drag coefficient vary in nearly sinusoidal manner with the amplitudes proportional to the velocity amplitude and with no apparent shift of phase, whereas for $\Delta U \gtrapprox 1.0$ the waveform of N_{um} is deformed at around the phase of the lowest flow velocity. The amplitude of the fluctuating flow velocity affects then not only the amplitudes of $\tilde{N}_{um}$ and $\tilde{C}_D$ but also their time-mean value $\bar{N}_{um}$ and $\bar{C}_D$.

The variations of the amplitude of $\tilde{N}_{um}$ and $\tilde{C}_D$ with the amplitude of the fluctuating flow velocity are illustrated in figure 16, where the ordinates are the ratios of $\tilde{N}_{um}$ and $\tilde{C}_D$ for their quasi-steady values. At a low frequency ($F=0.025$), $\tilde{N}_{um}$ is kept nearly constant within 5% departure from the quasi-steady value for $\Delta U<0.4$, while in the high frequency case ($F=0.25$) it does not coincide with the quasi-steady value even for infinitesimal velocity amplitude.

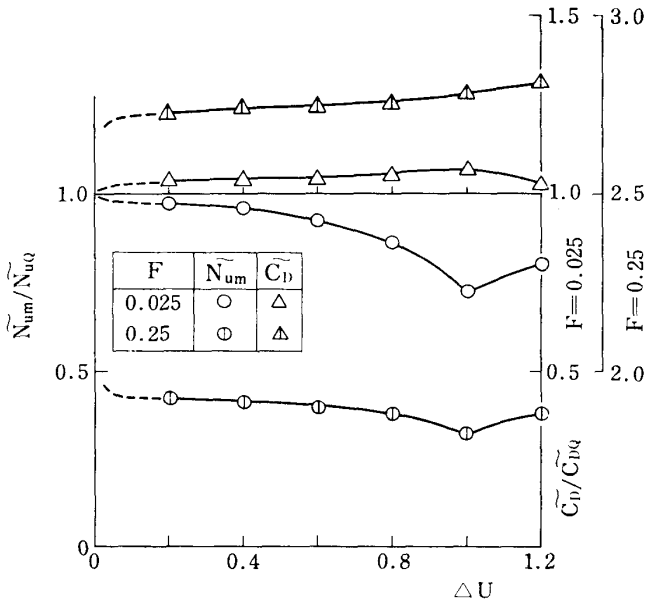

FIG. 16. Dependence of average Nusselt number and drag coefficient on the amplitude of fluctuating flow velocity. $Re=4$.

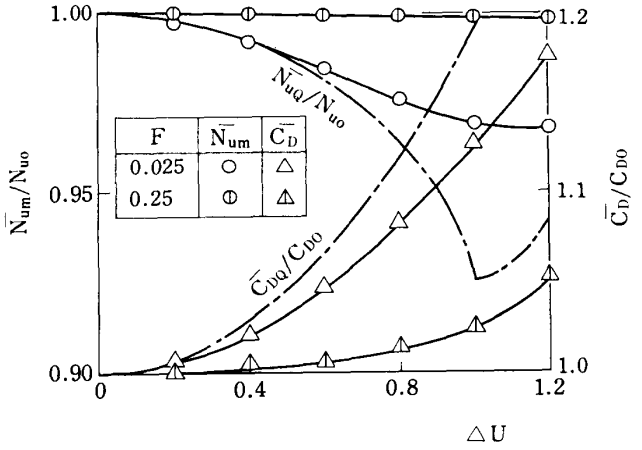

FIG. 17. Dependence of the time-mean values of average Nusselt number and drag coefficient on the amplitude of fluctuating flow velocity. $Re=4$.

The drifts of the time-mean values, $\bar{N}_{um}$ and $\bar{C}_D$, as a function of the velocity amplitude are presented in figure 17, where the ordinates are the ratios for the steady quantities, N_{u0} and C_{D0}. The dot-dash lines correspond to the time-mean values presumed from the quasi-steady variations as the ratios of the steady values. At $F=0.025$, $\bar{N}_{um}$ decreases coincidently with $\bar{N}_{uQ}$ as ΔU increases up to 0.4, whereas for $\Delta U>0.4$ the drift of $\bar{N}_{um}$ becomes smaller than that of $\bar{N}_{uQ}$, because the deformation of the waveform due to the reversed flow suppresses the further drift of $\bar{N}_{um}$. The drifts of $\bar{N}_{um}$ and $\bar{C}_D$ for higher frequency are mucch smaller than those for the lower frequency.

5. Conclusion

Some fundamental studies concerning the dynamic characteristics of the constant-temperature hot-wire were carried out by a numerical calculation from the thermo-fluiddynamic point of view. Solving the vorticity and energy equation, obtained are the flow and temperature fields around a heated circular cylinder in fluctuating flows for the time-mean flows of $Re=4$ and 40. The drag force and the rates of heat transfer from the cylinder are then determined. Their dependence on the amplitude and frequency of flow fluctuations are discussed, remarking the validity of the quasi-steady approximation.

For smaller amplitude of fluctuating flow velocity such as 20% fluctuation, the quasi-steady approximation may hold in the ordinary Reynolds number and frequency ranges for which the hot-wire is usually applied.

For larger amplitude of fluctuating flow velocity, however, the situation becomes surprisingly different. During a part of the cycle, the hot-wire may be embedded occasionally by the reversed wake flow, and hence the waveform of the average Nusselt number is much deformed such that the quasi-steady approximation should be abandoned even in rather low frequency range. It should be noticed that such deformed signals from the hot-wire can not be compensated by usual electronic methods and may lead to the misunderstandings of the phenomena even when no apparent reverse flow exists.

Department of Propulsion
Institute of Space and Aeronautical Science
University of Tokyo
November 2, 1978

References

Apelt, C. J., 1961 *Rep. & Mem., Aeron. Res. Council*, 3175.
Hinze, J. O., 1959 *Turbulence*, 76, McGraw-Hill.
Howarth, L. (ed.), 1953 *Modern Developments in Fluid Dynamics, High Speed Flows*. Oxford University Press.
Ishigaki, H., 1970 *J. Fluid Mech.*, 43-3, 477.
Ishigaki, H., 1972 *J. Fluid Mech.*, 56-4, 619.
Keller, H. B. and Takami, H., 1966 *Proc. Symp. on Numerical Solution of Nonlinear Differential Equations, University of Wisconsin.*
Lighthill, M. J., 1954 *Proc. Roy Soc. London*, Ser. A, 224, 1.
McAdams, W. H., 1954 *Heat Transmission*. 3rd ed., McGraw-Hill.
Mori, Y. and Tokuda, S., 1966 *Trans. Japan Soc. Mech. Enggrs.*, 32-239, 1100.
Okajima, A., Takata, H. and Asanuma, T., 1971 *Trans. Japan Soc. Mech. Enggrs.*, 37-307, 2300.
Tritton, D. J., 1959 *J. Fluid Mech.*, 6-4, 547.